Hindawi
Journal of Nanomaterials
Volume 2018, Article ID 9167938, 13 pages
https://doi.org/10.1155/2018/9167938

Research Article

The Effect of Temperatures on the Synergistic Effect between a Magnetic Field and Functionalized Graphene Oxide-Carbon Nanotube Composite for Pb^{2+} and Phenol Adsorption

Li-li Jiang,[1] **Hai-Tao Yu**,[2] **Lie-fei Pei**,[1] **and Xin-gang Hou**[1]

[1]*School of Material Science and Technology, Lanzhou University of Technology, Langongping Road, Lanzhou, Gansu 730050, China*
[2]*Department of Medical Laboratory, The First Hospital of Lanzhou University, No. 1, Donggang Road, Chengguan District, Lanzhou, Gansu 730000, China*

Correspondence should be addressed to Li-li Jiang; jianglili2002@163.com

Received 12 April 2018; Accepted 12 July 2018; Published 30 July 2018

Academic Editor: Oscar Perales-Pérez

The effect of temperature on scale inhibition and adsorption properties for Pb^{2+} and phenol was studied under the synergistic effect of the magnetic field and the adsorbent. The sulfhydryl and amino-modified graphene oxide/oxidized multiwalled carbon nanotubes (NH_2-SH-GO/o-MWCNTs) were synthesized and applied as the adsorbent. Additionally, changes in pH, conductivity, molecular activation energy, the relative variation of intramolecular energy and the relative variation in the proportion of free water, and adsorption capacity of the adsorbent were studied under different temperatures of circulating water. The relative variation of the proportion of free water increased with the increasing temperatures. The above results indicated that higher temperature would be detrimental to scale inhibition. The higher the temperatures, the lower the intramolecular energies. And the more stable molecules are formed in the circulating water. Thus, the results reduced the tendency to scale formation. The increased temperatures promoted the adsorption capacity of the adsorbent for Pb^{2+} and phenol. The adsorption process for Pb^{2+} and phenol conformed to the pseudo-second-order kinetic model and Freundlich isotherm model under the synergistic effect of magnetic field and NH_2-SH-GO/MWCNTs. After five cycles, the adsorption capacities of the adsorbent for Pb^{2+} and phenol separately decreased by 59.86% and 76.36%. The aforementioned results reveal that temperatures can promote the adsorption process for Pb^{2+} and phenol, and the synergistic effect between magnetic field and the adsorbent has a potential application for water treatment.

1. Introduction

Water resources play a crucial role in the development of the population, society, and economy. However, water resources in China in recent years faced two serious problems: water shortage and water pollution [1–3]. Water pollution can be divided into three types, that is, physical, biological, and chemical pollutions according to the types of pollutants. Heavy metal and organic pollutions belonging to chemical pollution have particularly serious harm [4]. The process of industrial production is generally accompanied with the discharge of large amounts of wastewater containing heavy metals and phenol. If the wastewater is discharged without treatment, it will flow into ecological waters to exert baneful influences and harms to the natural environment and human health. Heavy metal ions are nondegradable and highly stable, so they cannot be treated like organic pollutants through natural degradation or photo-catalytic degradation [5]. Their forms and locations can only be changed using physical or chemical means, for example, precipitating heavy metal ions using acid or alkaline solvents or adsorbing and accumulating them using adsorbents. As heavy metal ions are of high economic value, treating heavy metal pollution cannot only alleviate the environmental pollution but also recycle heavy metals [6]. For this reason, the control over heavy metal pollution has great research prospects. Lead ion is one of the toxic heavy metal ions causing water pollution. Lead ion in water pollutants mainly comes from

the substandard discharge of industrial wastewater, such as the discharge of lead-containing wastewater generated in the processes of mineral mining and industrial production of electroplating industry and battery industry. Having serious harm to human health, lead ion can stay in human body for more than 25–35 days [7]. Phenol can also severely impair multiple organs in the human body. When organisms contact with low-dose phenol for a long time, it is likely to induce carcinogenesis and lead to other harms such as malformation of organs [8]. So, we choose the Pb^{2+} and phenol as the research project.

At present, there are mainly three methods for treating heavy metal and phenolic pollutants, that is, chemical precipitation, microbiological method, and physical treatment. Chemical precipitation relies on the chemical reaction between heavy metal ions and treating agents to produce insoluble precipitates and then separates the precipitated products through filtration or other means. While chemical treatment methods need low operation cost and are simple in operation, they call for large quantities of treating agents in the treatment process [9]. In addition, the improper use of treating agents may cause secondary pollution. Microbiological treatment of heavy metal and phenolic pollutants depends on large amounts of groups of phosphate and carbonyl compounds on the surface of microorganisms such as bacteria and fungi. These groups have strong coordinating and chelating ability with heavy metals and phenols. At the same time, microorganisms can also treat wastewater containing heavy metal ions and phenols by means of bioaccumulation and metabolism. However, microbiological treatment methods also have many shortcomings, such as small adsorption capacity. Moreover, each microorganism can only adsorb a single heavy metal ion or phenol, so they show poor treatment effects on mixed wastewater containing multiple heavy metal ions and phenols [10]. In comparison, physical treatment methods are important approaches for dealing with wastewater containing heavy metal ions and phenols. Physical treatment methods mainly include membrane separation, ion exchange method, and adsorption method. Among them, the adsorption method is one of the most commonly used treatment methods for wastewater and the most important water treatment method [11]. Therefore, adsorption method is more and more widely used in water purification and more studies are carried out to improve the performance of adsorbents and develop new adsorbents.

Ever since being discovered, carbon nanotubes (CNTs) and graphene have attracted attentions from plenty of researchers. In addition, huge amounts of CNTs and graphene have been studied and used to develop new adsorbents. Li et al. oxidized the original CNTs using H_2O_2, HNO_3, and $KMNO_4$, respectively, to adsorb Cd^{2+} [12]. The comparative experiments showed that the oxidization treatment is able to effectively improve the adsorption capacity of CNTs for Cd^{2+} and produce many oxygen-containing groups, such as carboxyl and hydroxyl, on the surface of the original CNTs. They also pointed out that pH is an important factor influencing the adsorption of CNTs. Saleh and Gupta prepared a kind of MnO_2-coated CNT composite (MnO_2/CNT) to be used for adsorbing Pb^{2+} [13]. They found that MnO_2/CNT has the highest removal rate for Pb^{2+} at the pH of 6~7 and that increasing the thickness of MnO_2/CNT layer and reducing the flow rate of the fixed bed are able to significantly improve the adsorption rate. Hadavifar et al. [14] selected ethylene diamine, cyanuric chloride, and 2-mercaptoethanol sodium to react with multiwalled CNTs successively and successfully loaded amino and thiol functional groups on the sidewalls of the multiwalled CNTs. In this way, they prepared a new functional adsorption material. The results showed that the composite exhibits excellent adsorption capacity for Hg^{2+}. Under conditions of pH = 6 and 400 mg/L of the adsorbent, the adsorption capacity for Hg^{2+} is as high as 105.65 mg/g. After five cycles of adsorption and desorption, the adsorption capacity can still remain above 92.8%. Jiang et al. [15] uniformly loaded Fe_3O_4 nanoparticles on the surface of CNTs using the hydrothermal method, and the prepared composite was used to adsorb Pb^{2+} and Zn^{2+} in water. The experimental results showed that the magnetic CNT composite had considerable adsorption capacity for Pb^{2+} and Zn^{2+}, and the equilibrium adsorption capacities for the two ions can reach 67.25 and 3.759 mg/g, respectively. The results indicate that the magnetic CNT composite has great potential as a high-performance adsorbent.

Magnetic treatment has been extensively used in the water treatment field due to its various advantages including no secondary pollution, compact equipment, one-time investment, and low operation cost [16]. With the in-depth study on magnetic treatment, the combination of magnetic treatment and adsorption has become a new research focus. Li et al. [17] conducted the adsorption experiments for Cr^{2+} using the modified chitosan together with the magnetic field. The results demonstrated that the use of magnetic field is able to improve the adsorption capacity of the modified chitosan for Cr^{2+}. The equilibrium adsorption capacity increased from 0.43 to 0.94 mg/g, and the adsorption time was shortened remarkably. Li et al. studied the influences of magnetic field on the adsorption of biocarbon produced from straw of wheat for methylene blue [18]. Due to the application of the magnetic field, the equilibrium adsorption capacity for the dye grew from 46.6 to 62.5 mg/g. To the best of our knowledge, a technique combining the use of a magnetic field and GO/CNT has not been reported to date.

The present study aims to study how temperature influences on synergistic effect between the magnetic field and the adsorbent. The scale inhibition of circulating water and adsorption properties of adsorbents for Pb^{2+} and phenol were studied. The new adsorbent sulfhydryl- and amino-modified GO/oxidized multiwalled carbon nanotubes (NH_2-SH-GO/o-MWCNTs) was prepared. Various parameters were determined including the equilibrium adsorption capacity of the adsorbent, the pH, conductivity, molecular activation energy, and the relative changes in the intramolecular energy and proportion of free water. To reduce the cost of using the adsorbent in practical applications, experiments were carried out to investigate the cycle times and to investigate the interaction between adsorbents and adsorbates by X-ray photoelectron spectroscopy (XPS).

2. Experiment and Methods

2.1. Materials and Reagents. MWCNTs were purchased from Chengdu Organic Chemistry Institute of Chinese Academy of Sciences (China). According to the manufacturer, the diameters of the MWCNTs are in the range from 10 to 20 nm and their specific surface areas vary from 100 to 160 m^2/g. Lead nitrate and phenol were purchased from Tianjin Fu Rui Technology Co. Ltd. (China). Nitric acid, sulphuric acid, and hydrazine (F > 99.5%) were purchased from Big Alum Chemical Reagent Factory (China). The (3-mercaptopropyl)trimethoxysilane (MPTS) was purchased from Beijing Biological Technology (China). All of the chemicals were of analytical grade and used without further purification.

2.2. Characterization Techniques. The pH value of water sample was measured using pH meter (Delta320, Mettler Toledo instrument). The electrical conductivity meter (Delta326, Mettler Toledo instrument) was used to measure the electrical conductivity of water sample. Nuclear magnetic resonance spectrometer (Bruker Avance AVIII 400) was used to determine the relative variation in the proportion of free water. Viscosity is analyzed with a viscometer produced by Shanghai Fangrui Devices Co. Ltd. The liquid viscosity η (mPa·s) can be used to calculate the variation of activation energy. Surface tension was measured by two-capillary electronic balance to calculate the relative variation of intramolecular energy. XPS (Escalab 250Xi with a max resolution of 400,000 cps) was applied to determine the chemical composition of the sample surface using AlK radiation. The XPS spectra were analyzed using XPS peak software. According to the obtained peak areas, the surface atomic percentages were calculated. The concentration of lead ions was analyzed using a Hitachi Z-5000 atomic absorption spectrophotometer (AAS), and that of phenol was obtained with an ultraviolet-visible spectrophotometer (model VU-1000). All of the water in the experiment was produced using an ultrapure water system (UPD-I-20T).

2.3. Preparation of NH_2-SH-GO/o-MWCNTs. 0.2 g of GO and 0.4 g of o-MWCNTs were dispersed in 200 mL of absolute alcohol and treated for 4 h with ultrasound, then the above mixture was filtered and washed with ultrapure water for several times. The above mixture was dried in a vacuum oven for 12 h at 80°C. The obtained product is GO/o-MWCNTs. A weight of 100 mg GO/o-MWCNTs was dispersed in 20 mL of absolute alcohol at 25°C and treated for 4 h with ultrasound. Then, 2 mL of acetic acid and 4 mL of MPTS were added in the above mixtures and the solution was stirred for 24 h. The mixture was filtered and washed for several times with ultrapure water. The obtained product is SH-GO/o-MWCNTs. Then, 100 mg of SH-GO/o-MWCNTs was dispersed in 50 mL of absolute alcohol and stirred for 12 h, and 10 mL of hydrazine hydrate was added in the above mixtures. Finally, the product was dried in a vacuum oven at 80°C for 8 h. The product finally obtained was NH_2-SH-GO/o-MWCNTs.

2.4. Influence of Temperatures on Scale Inhibition and Adsorption Performance. 10 L of configured solutions was added into the circulating water system, and the flow velocity (0.17 m/s), magnetic field intensity (0.54 T), and temperatures (10°C, 20°C, 25°C, 30°C, and 40°C, resp.) were adjusted. Our previous experiment results showed that the effect was the best under the condition. The configured solution containing Ca^{2+}, Pb^{2+}, and phenol at the initial concentration of 50 mg/L separately was prepared. The magnetic treatment and adsorption experiment were conducted after starting the circulating water system in which the NH_2-SH-GO/o-MWCNTs with an initial concentration of 50 mg/L (prepared in advance) was added. Afterwards, the pH, conductivity, viscosity, and surface tension of the solution at 5, 15, 25, 35, 45, 60, 75, 100, 140, 195, 285, 405, 525, and 685 min were measured. On this basis, the water quality indexes, that is, relative variation of intramolecular energy and the variation of molecular activation energy, were calculated. Additionally, small water specimens were taken separately at 0 min and 685 min to measure the peak width at half height of the circulating water by using a nuclear magnetic resonance (NMR) spectrometer. By doing so, the variation of the proportion of free water molecules in circulating water was further calculated.

The relative variation of intramolecular energy mainly depends on the surface tension, calculated as follows [19]:

$$\frac{E^{\text{Inner}} - E_0^{\text{Inner}}}{E_0^{\text{Inner}}} = \frac{\Delta E}{E_0} = \frac{T - T_0}{T_0}, \tag{1}$$

where E^{Inner} refers to the intramolecular energy (J) and T refers to surface tension (N/m). As before, a subscript "0" refers to an initial value (before application of the magnetic field) and unsubscripted values to those after magnetic treatment. Thus, $(E^{\text{Inner}} - E_0^{\text{Inner}})/E_0^{\text{Inner}}$ represents the relative change in intramolecular energy caused by the magnetic field.

The variation of activation energy is determined according to the viscosity, calculated as follows [20]:

$$\Delta E' = -RT \ln\left(\frac{\eta}{\eta_0}\right) = E' - E_0', \tag{2}$$

where ΔE' refers to the variation of activation energy, E' and $E_0{}'$ represent the molar activation energies (J/mol) of the experimental and control (ultrapure water) groups, respectively, R represents gas constant (J/(mol·K)), and T means temperature (K). Additionally, η and η_0 refer to the viscosities of the experimental and control groups, respectively.

The relative variation in the proportion of free water molecules depends on the quantities of hydrogen bonds in the circulating water, which can be measured by using the peak width at half height from NMR spectrometric data, calculated as follows [21]:

$$\frac{\Delta C}{C_0} = \frac{C - C_0}{C_0} = \frac{\Delta \nu_{1/2}^0 - \Delta \nu_{1/2}}{\Delta \nu_{1/2}}, \tag{3}$$

where C is the proportion of free water after magnetic treatment, C_0 is the proportion of free water without magnetic field, and $\Delta C/C_0$ is the relative variation in the proportion of free water. In addition, $\Delta\nu_{1/2}$ is the experimental peak width at half height under magnetic field and $\Delta\nu_{1/2}^0$ is the initial peak width at half height without magnetic field.

Afterwards, a certain amount of circulating water was taken to measure the concentrations of Pb^{2+} by atomic absorption spectrophotometry and the concentration of phenol by using ultraviolet-visible spectrophotometry. Furthermore, the adsorption capacities of the adsorbent for Pb^{2+} and phenol were calculated. The adsorption capacity (q_t) of the adsorbent can be calculated using the following formula [22]:

$$q_t = \frac{(C_0 - C_e)V}{m}, \tag{4}$$

where q_t is the quantity adsorbed by the adsorbent at time t (mg/g); C_0 and C_e are the initial and equilibrium concentrations of adsorbate (mg/L), respectively; V is the volume of the solution (L); and M is the mass of adsorbent (g). The experimental data for adsorbing Pb^{2+} and phenol were fitted by using pseudo-first-order and pseudo-second-order kinetic models. The pseudo-first-order kinetic equation can be expressed as follows [23]:

$$\ln(q_e - q_t) = \ln q_e - k_1 t, \tag{5}$$

where q_e and q_t refer to the adsorption capacities (mg/g) of the adsorbents under adsorption equilibrium and at time t, respectively. Moreover, k_1 and t represent the rate constant (min^{-1}) of the pseudo-first-order kinetic equation and time (min), respectively. According to the pseudo-first-order kinetic equation, a graph was drawn for t by using $\ln(q_e - q_1)$ and the slope of the resulting line was the rate constant k_1. The pseudo-second-order kinetic equation is given by [24]:

$$\frac{t}{q_t} = \frac{1}{k_2 q_e^2} + \frac{t}{q_e}, \tag{6}$$

where k_2 refers to the rate constant (g/mg/min) of the pseudo-second-order kinetic equation. The values of t/q_t were plotted against t, and then the values of parameters q_e and k_2 can be calculated by using the slope and intercept of the obtained straight line.

Langmuir and Freundlich isotherm models were the most common models to describe the adsorption process. Langmuir isotherm model is mainly used to describe uniform, monolayer adsorption process. Freundlich isotherm model assumes that the adsorption process occurs on the surface of an inhomogeneous medium. Langmuir isotherm model is given by [25]

$$\frac{1}{q_e} = \frac{1}{bq_m C_e} + \frac{1}{q_m}, \tag{7}$$

where C_e and q_e refer to the concentration (mg/L) of metal ions and equilibrium adsorption capacity (mg/g) of the adsorbent under adsorption equilibrium, respectively. The graph of $1/C_e$ was drawn by using $1/q_e$, and then the adsorption constant b and parameter q_m can be obtained according to the slope and intercept of obtained straight line. The Freundlich isotherm model is given by [26]

$$\ln q_e = \ln k_f + \frac{1}{n} \ln C_e, \tag{8}$$

where q_e and C_e represent the adsorption capacity (mg/g) of the adsorbent and the concentration of adsorbates (mg/L) at equilibrium, respectively. k_f and n refer to constants related to adsorption capacity and adsorption strength, respectively.

To investigate the adsorption mechanism of NH_2-SH-GO/MWCNTs for Pb^{2+} and phenol, a thermodynamic analysis was undertaken using the experimental results. The value of K_d was calculated by using (9). The linear fitting was conducted by separately taking $1/T$ and $\ln K_d$ as x- and y-coordinates to further calculate the enthalpy change (ΔH^0) and entropy change ($\Delta S0$) according to the slope and intercept of the straight line. Then, the variation of Gibbs free energy ΔG^0 can be calculated based on (11) [27].

$$K_d = \frac{(C_0 - C_e)V}{mC_e}, \tag{9}$$

$$\ln K_d = \frac{\Delta S^0}{R} - \frac{\Delta H^0}{RT}, \tag{10}$$

$$\Delta G^0 = \Delta H^0 - T\Delta S^0, \tag{11}$$

where R is the universal gas constant (8.314 J/mol/K), T is the adsorption temperature (K), and K_d represents the equilibrium constant obtained by the initial and the equilibrium concentrations (C_0 and C_e) of the target ions.

2.5. The Recycle Times of Adsorbent. The solution (100 mL) containing Pb^{2+}, Ca^{2+}, and phenol with an initial concentration of 50 mg/L was prepared. The pH value of the solution was adjusted to 5 by employing 0.1 mol/L HCl and NaOH solution. NH_2-SH-GO/MWCNTs at a concentration of 50 mg/L had been added to the above solution at 25°C. Then, the mixtures was put in the oscillation box to shake for 685 min. The mixtures were filtered by using acetylcellulose films with a pore size of 0.45 μm. Afterwards, the concentrations of Pb^{2+} and Ca^{2+} were measured by applying the atomic absorption spectrophotometer, and the concentration of phenol was measured by using the ultraviolet-visible spectrophotometer. The initial solution used for the experiment was taken as the blank control. The filtered NH_2-SH-GO/MWCNTs were immersed into 1% HCl for 1.5 h and washed until pH = 7 by using deionised water. The dried NH_2-SH-GO/MWCNTs were continuously subjected to cyclic adsorption-washing-adsorption. Under the aforementioned conditions, experiments were performed five times. The concentration of the solution was measured after each cycle to calculate the changing adsorption capacities.

3. Results and Discussion

3.1. Influence of Temperature on Water Quality Index. Temperature is an important factor influencing the

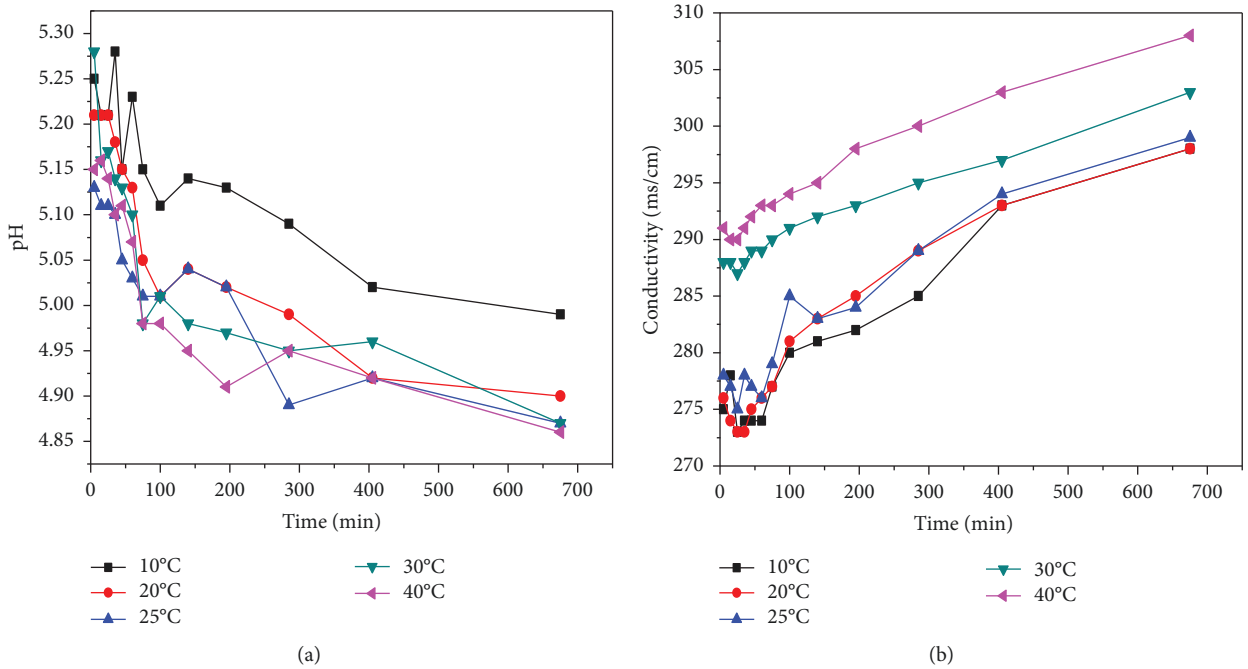

Figure 1: Influence of temperature on pH and conductivity.

synergistic effect between magnetic field and NH_2-SH-GO/o-MWCNTs. Therefore, the influence of temperatures on water quality index and adsorption capacity at 10°C, 20°C, 25°C, 30°C, and 40°C was investigated under a magnetic field intensity of 0.54 T, flow velocity of 0.17 m/s, and an initial concentration of 50 mg/L.

3.1.1. Influence of Temperature on pH and Conductivity. Figure 1 shows the changes of pH and conductivity with time at different temperatures: the pH value of the circulating water at 10°C first decreased and then tended to be stable. As the temperature increased, the pH also decreased at first and then stabilised. Moreover, pH values at different temperatures were similar, implying that the increased temperature exerted no significant influence on pH value. It can be speculated from Figure 1(b) that the conductivity of circulating water at 10°C gradually increased with increasing magnetic treatment time. Due to the magnetic field intensity at 0.54 T in this experiment, the presence of magnetic field was conducive to increasing the number of ions in the circulating water. Additionally, the change in conductivity increased with rising temperatures, which indicated that the higher the temperature, the greater the ionisation degree of the circulating water. Under these conditions, the ion mobility rate increased, which increased the conductivity. This suggested that more conductive ions were formed in the circulating water. Scale-forming ions were combined with water molecules to produce hydrated molecules, thus reducing the production of scale [28].

3.1.2. Influence of Temperature on the Relative Variation of Intramolecular Energies and Variation of Molecular Activation Energies. Figure 2 shows the changes in relative variation of intramolecular energies and the variation of molecular activation energies with time at different temperatures. Figure 2(a) shows that the activation energies in circulating water undergoing magnetic treatment gradually increased with time. The activation energies exhibited a similar change as the temperature increased. And the magnitude of the change was unconspicuous, implying that temperature had an insignificant influence on activation energy. The relative variation in intramolecular energies in the circulating water at 10°C decreased over time. The higher the temperature was, the more significant in relative variation of intramolecular energies were: it also indicated that the higher the temperature, the lower the intramolecular energies and the more stable molecules in the circulating water, thus reducing the tendency to scale formation.

3.1.3. Influence of Temperature on Relative Variation of Free Water Proportion. Figure 3 shows the change of the relative variation of free water proportion at different temperatures: the relative variation of free water proportion in the circulating water at 20°C was −27.16%. This implied that the relative variation of free water proportion in circulating water undergoing magnetic treatment at 685 min decreased by 27.16% compared with that in circulating water without magnetic field. The relative variations of free water proportions in the circulating water at 25°C, 30°C, and 40°C decreased by 21.15%, 6.227%, and 3.922%, respectively. The results revealed that the proportion of free water increased with increasing temperature because the increase of temperature accelerated the thermal motion of water molecules, thereby increasing the quantity of hydrogen bonds and the proportion of free water [29]. Therefore, the increase of temperature impaired the scale-inhibiting benefit of the synergistic effect between the magnetic field and NH_2-SH-GO/o-MWCNTs.

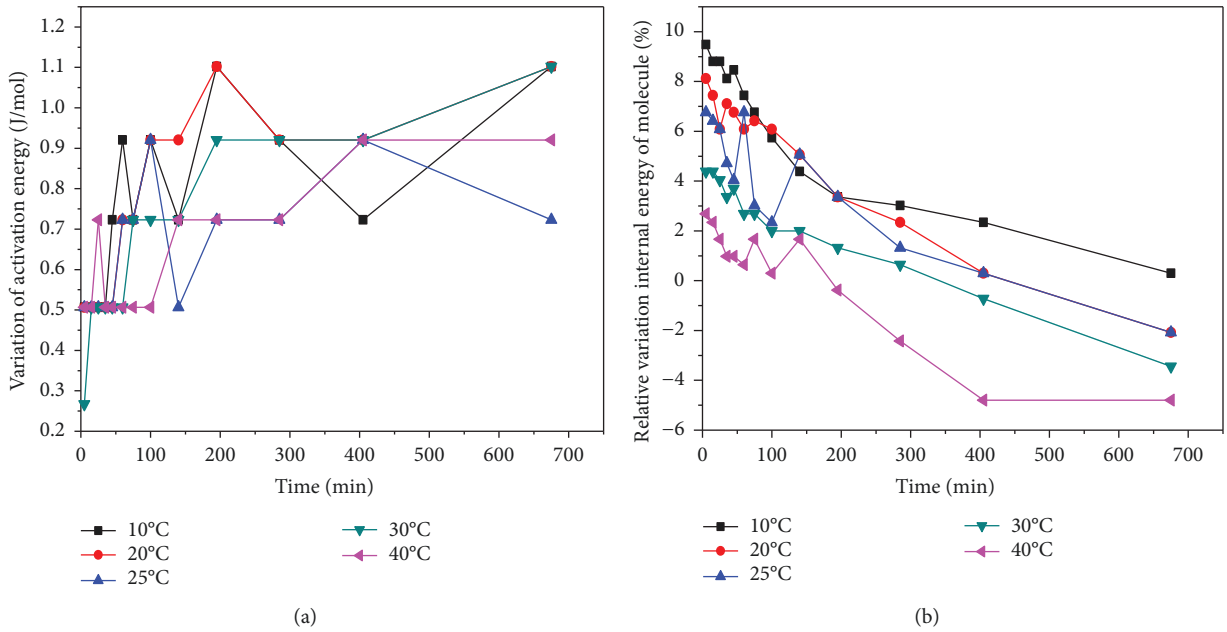

Figure 2: Influence of temperature on activation energy variation and relative variation internal energy of molecule.

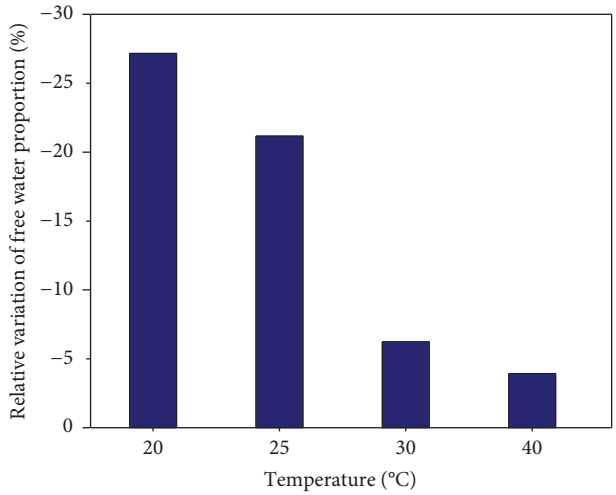

Figure 3: Influence of temperature on the relative variation of free water proportion.

3.2. Influence of Temperature on Adsorption Capacities

3.2.1. Influence of Temperature on Adsorption Capacities and Reaction Kinetic. Figure 4 shows the changes in adsorption capacities of the adsorbent at different temperatures over time: the adsorption capacity rapidly increased at first and then tended to stabilize over time for lead ion, as shown in Figure 4(a). The adsorption capacity for lead ion in circulating water at 20°C for 60 min was 101.89 mg/g. The equilibrium adsorption capacity of the adsorbent for lead ions in circulating water at 40°C was 131.27 mg/g. With the increased temperature of the circulating water, the adsorption rate and adsorption capacity of the adsorbent for lead ions both increased significantly, implying that the increased temperature promoted the adsorption capacity of the adsorbent for lead ions. With increasing temperature, the motion of ions or molecules increased in the circulating water, resulting in their increased kinetic energy. Therefore, the movement rate of lead ions to the surface of the adsorbent accelerated to increase the adsorption capacity of the adsorbent for lead ions. On the other hand, the increased temperature enhanced the activities of amino, sulfhydryl, and oxygen-containing groups on the surface of the adsorbent. As a result, the contact probability of ions with groups on the surface of the adsorbent improved to increase the adsorption capacity for lead ions. As shown in Figure 4(b), the adsorption rate and adsorption capacity of the adsorbent for phenol both greatly increased with increasing temperature; however, the equilibrium adsorption capacity for phenol was far lower than that for lead ions, which was mainly because there was a competitive relationship between lead ions and phenol during the adsorption process. The adsorption capacity first increased rapidly, and then the growth rate decelerated at 60 min. The adsorption capacity remained unchanged after 60 min when it reached an equilibrium state. The equilibrium adsorption capacity of the adsorbent for phenol in circulating water at 40°C was 35.79 mg/g.

The adsorption processes at different temperatures were fitted by using Lagrange pseudo-first-order and pseudo-second-order kinetic equations. The fitting result obtained by using pseudo-second-order kinetic equation is shown in Figure 5, and the parameters are displayed in Table 1. It can be seen from Table 1 that the adsorption processes of NH_2-SH-GO/o-MWCNTs at different temperatures for Pb^{2+} and phenol conformed to the pseudo-second-order kinetic model ($R^2 = 0.999$): this indicated that the adsorption rate was positively correlated with the concentrations of the two adsorbates. As the temperature increased, the equilibrium adsorption capacities of NH_2-SH-GO/o-MWCNTs for

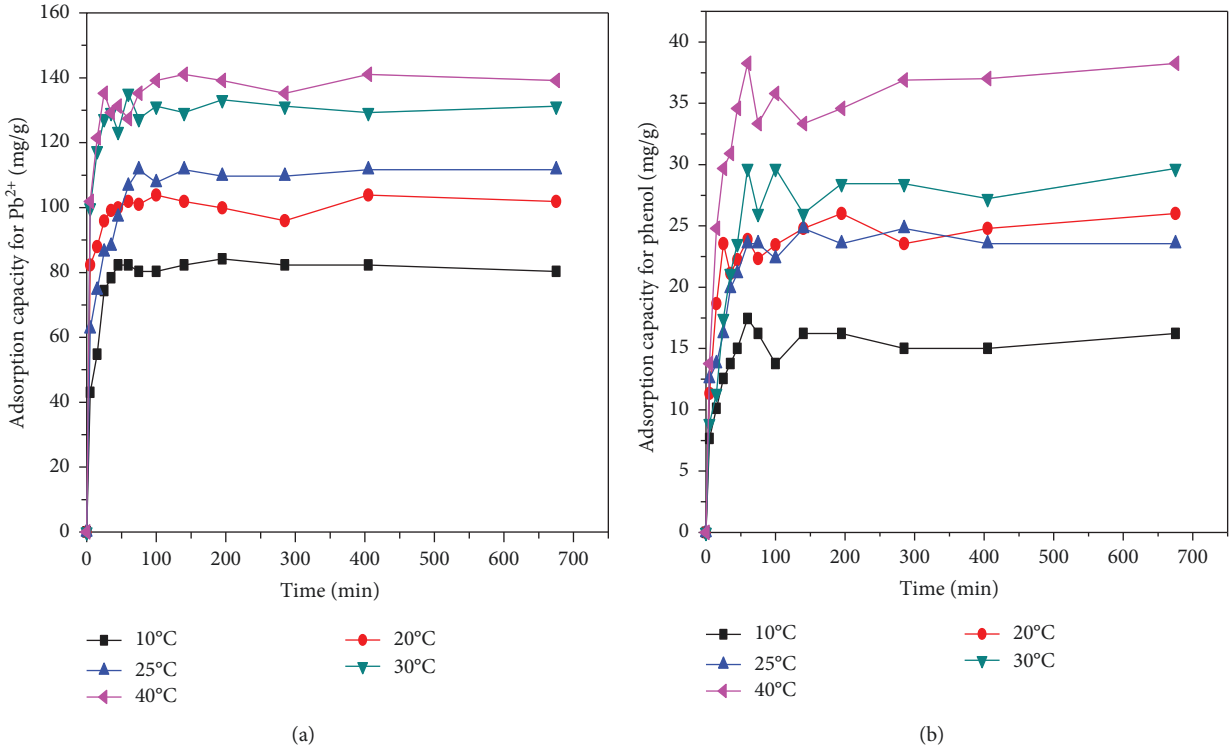

Figure 4: Influence of temperature on adsorption capacity: (a) Pb^{2+}; (b) phenol.

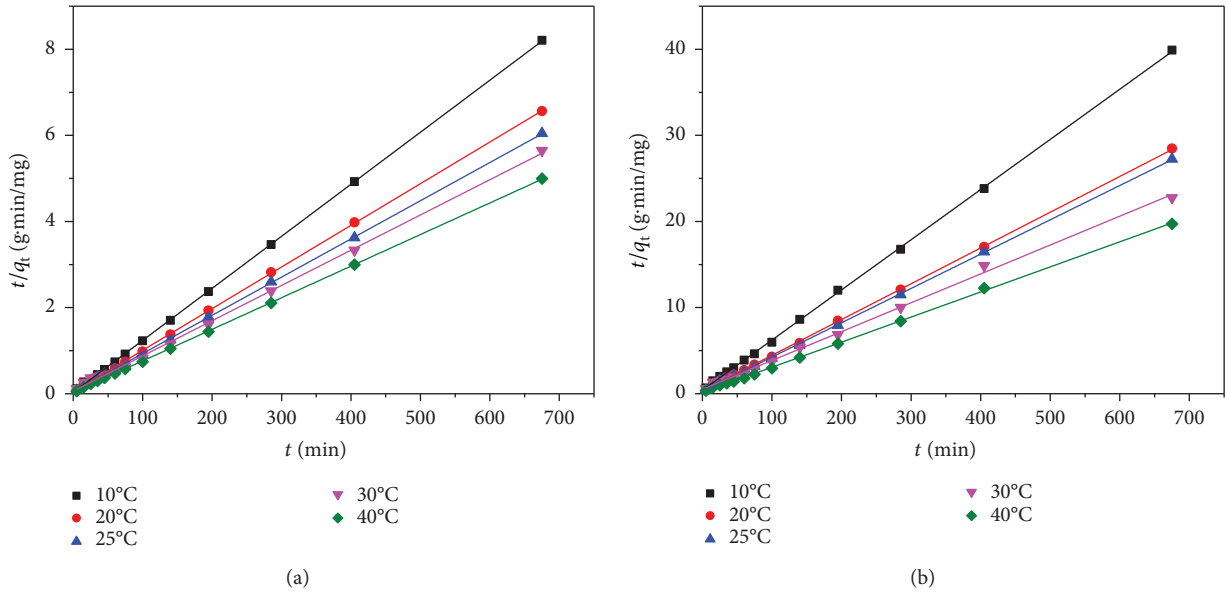

Figure 5: Pseudo-second-order kinetic model for (a) Pb^{2+} and (b) phenol at different temperatures.

Pb^{2+} and phenol gradually increased, implying that the increasing temperature promoted the adsorptions of the adsorbent. It can also be speculated from Table 1 that the adsorption rate constant k_2 for lead ions was close to that for phenol, which suggested that the adsorption rate of the adsorbent for Pb^{2+} was the same as that for phenol. With increasing temperature, the adsorption rate constants for lead ions and phenol both decreased, indicating that the higher the temperature, the lower the adsorption rate constants. The result showed that increasing water temperatures reduced the adsorption rates of NH_2-SH-GO/o-MWCNTs for Pb^{2+} and phenol. Additionally, h refers to the initial adsorption rate for adsorbates at 0 min. As shown in Table 1, the initial adsorption rate of NH_2-SH-GO/o-MWCNTs for Pb^{2+} was far larger than that for phenol, which was consistent with the fact that the adsorption

Table 1: Fitting results of adsorption kinetics under different temperatures.

Adsorbate	Temperature	Pseudo-first-order model			Pseudo-second-order model				
		$q_{ca,e}$ (mg·g^{-1})	k_1 (min^{-1})	R^2	$q_{ex,e}$ (mg·g^{-1})	$q_{ca,e}$ (mg·g^{-1})	h	k_2 (mg·g^{-1}·min^{-1})	R^2
Pb^{2+}	10	3.53	0.00967	0.758	82.31	82.71	32.84	0.0048	0.999
	20	9.88	0.00789	0.797	102.92	103.41	23.52	0.0022	0.999
	25	12.30	0.0106	0.779	111.70	112.74	21.61	0.0017	0.999
	30	6.35	0.0097	0.884	120.90	121.95	68.41	0.0046	0.999
Phenol	40	10.92	0.011	0.761	135.22	136.24	35.27	0.0019	0.999
	10	2.70	0.006	0.776	17.10	17.17	2.48	0.0084	0.999
	20	3.00	0.008	0.692	23.81	24.07	3.30	0.0057	0.999
	25	2.65	0.008	0.690	24.88	25.09	3.71	0.0059	0.999
	30	5.59	0.011	0.858	27.91	28.38	3.22	0.0040	0.999
	40	4.38	0.006	0.779	34.32	34.33	6.25	0.0053	0.999

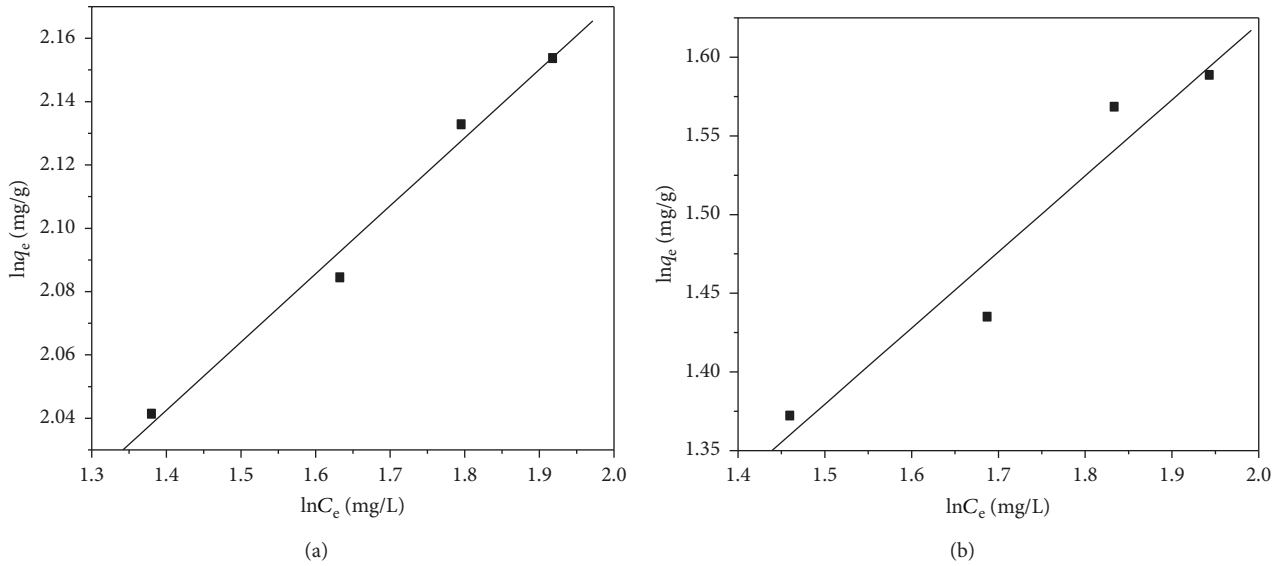

Figure 6: The fitting results of Freundlich model for Pb^{2+} (a) and phenol adsorption (b).

Table 2: Fitting parameters of Langmuir and Freundlich isotherm models.

Adsorbate	Langmuir isotherm model			Freundlich isotherm model		
	q_m (mg/g)	b (L/mg)	R^2	K_f (mmol^{1-n}·L^n/kg)	n	R^2
Pb^{2+}	131.6	0.27	0.989	55.12	4.65	0.993
Phenol	90.74	0.01	0.876	2.99	2.07	0.966

capacity of NH_2-SH-GO/o-MWCNTs for Pb^{2+} was larger than that for phenol.

3.2.2. Adsorption Isotherms. Examination of the adsorption isotherm is a typical method used to analyze adsorption data and to explore the mechanism. Langmuir and Freundlich isotherm models are generally used to investigate the adsorption mechanism. The adsorption process was fitted by employing Langmuir and Freundlich isotherm models, and the fitting results using the Freundlich isotherm model were shown in Figure 6. The parameters of the fitting results are listed in Table 2. According to the correlation coefficient R^2 in Table 2, the adsorption process of NH_2-SH-GO/o-MWCNTs for Pb^{2+} and phenol conformed to the Freundlich isotherm model. By taking the adsorption process for phenol as an example, the correlation coefficients of Langmuir and Freundlich models were 0.876 and 0.966, respectively. Therefore, the adsorption process of NH_2-SH-GO/o-MWCNTs for Pb^{2+} and phenol conformed to the Freundlich isotherm model as evinced by the correlation coefficient. This meant that phenol interacted with itself and the adsorbates, thus being a multilayer adsorption process, as was the case for

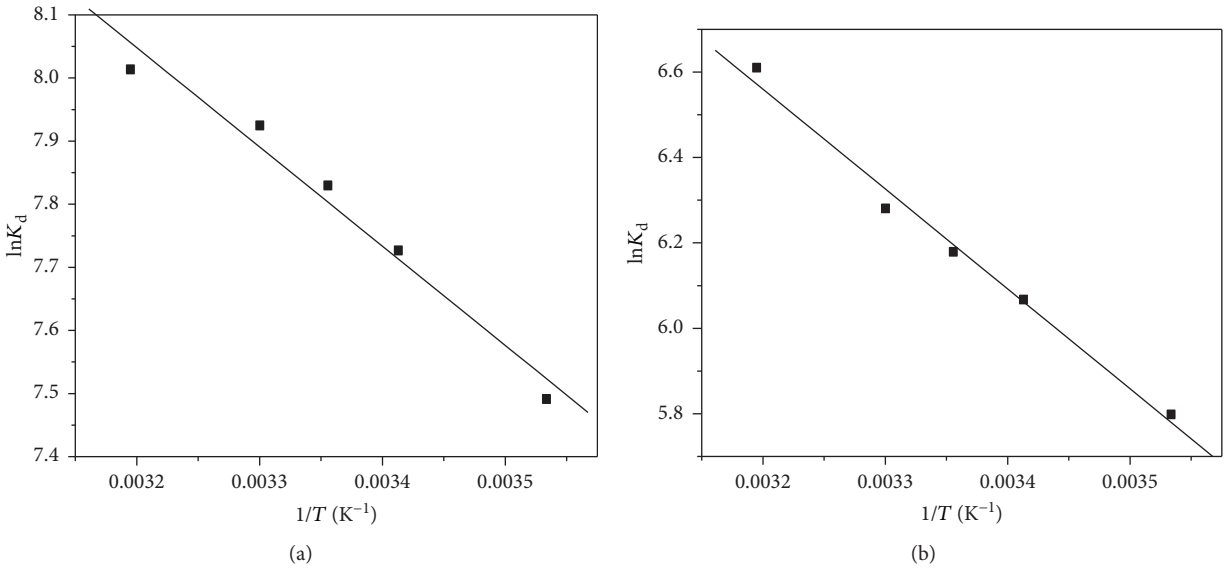

Figure 7: Linear fitting between ln K_d and $1/T$ for Pb^{2+} (a) and phenol (b).

the adsorption of lead ions [30]. Additionally, the adsorption process occurred readily as the adsorption intensity constant n was within the range from 2 to 10. The adsorption intensity constant of Pb^{2+} ranged from 2 to 10 while that of phenol was around 2, which implied that the adsorption reaction of the adsorbent for Pb^{2+} and phenol occurred readily. Moreover, the value of K_f for Pb^{2+} during the adsorption process was larger than that for phenol, and the former was about 18 times than that of the latter, implying that Pb^{2+} was more easily adsorbed using the adsorbent so that the adsorption capacity for Pb^{2+} was larger than that for phenol.

3.2.3. Adsorption Thermodynamics. Temperature is an important parameter influencing the adsorption capacity under the synergistic effect of magnetic field and NH_2-SH-GO/o-MWCNTs. To determine the thermodynamic parameters, a thermodynamic study involving adsorption of lead ions and phenol at initial concentrations of 50 mg/L was conducted at 283, 293, 298, 303, and 313 K, respectively. The concentration of the adsorbent in each experimental specimen was set to 50 mg/L, and the adsorption lasted for 675 min. The corresponding thermodynamic parameters can be calculated according to (9), (10), and (11). By using the slope and intercept of the straight line in Figure 7, the values of enthalpy and entropy changes were calculated. Moreover, the Gibbs free energies at different temperatures can also be obtained according to (11), and the details are displayed in Table 3.

Table 3 revealed that the absolute value of Gibbs free energy gradually increased with increasing temperature. The value was negative, implying that the adsorption processes of NH_2-SH-GO/o-MWCNTs for Pb^{2+} and phenol were spontaneous. As the temperature decreased, the Gibbs free energies also decreased, which indicated that the adsorption process was effective at high temperatures, namely, increasing the temperature was conducive to the adsorption process. Additionally, according to the literature, physical, physico-chemical, and chemical adsorption processes occurred at −20~0, −20~−80, and −80~−400 kJ/mol, respectively [31]. Therefore, according to the calculated Gibbs free energy, the adsorption types of NH_2-SH-GO/o-MWCNTs for lead ions and phenol can be judged. Table 3 revealed that the adsorption processes of NH_2-SH-GO/o-MWCNTs for lead ions and phenol were physical processes. The functional groups on the surface of NH_2-SH-GO/o-MWCNTs (such as sulfhydryl and amino) can be combined with lead ions and phenol through Van der Waals' force or electrostatic attraction in water to improve the adsorption process. The enthalpy change was positive, which implied that the adsorption process was an endothermic process. The larger entropy change indicated that there was an obvious entropy change in the adsorption process during which the solid-liquid interface developed towards a more chaotic state. Entropy change occurred owing to water

Table 3: Thermodynamic parameters of adsorption process for Pb^{2+} and phenol.

	T (K)	Ln K_d	ΔG (kJ·mol^{-1})	ΔH (kJ·mol^{-1})	ΔS (J·mol^{-1}·K^{-1})
Pb^{2+}	283	7.491	−17.701	13.079	108.767
	293	7.726	−18.789		
	298	7.829	−19.333		
	303	7.924	−19.876		
	313	8.013	−20.964		
Phenol	283	5.798	−13.599	19.447	116.772
	293	6.067	−14.767		
	298	6.179	−15.350		
	303	6.280	−15.934		
	313	6.609	−17.102		

molecules being produced by ion exchange reaction, the affinity of NH_2-SH-GO/o-MWCNTs to lead ions and phenol, and the increasing randomness of the water interface in the adsorption process.

3.3. Recycling of the Adsorbent. To reduce the cost of using the adsorbent in practical applications, experiments were carried out to investigate the number of cycles through which the adsorbent could be used. Figure 8 shows that the adsorption capacities of the adsorbent for Pb^{2+} and phenol gradually declined with increasing use. The adsorption capacities of adsorbent for lead ions and phenol separately decreased to 99.90 mg/g and 22.34 mg/g after the first use, decreasing by 17.76% and 17.97%, respectively. This reduction in the adsorption capacity was because amino, sulfhydryl, and oxygen-containing groups on the surface of the adsorbent were removed by acid and water after undergoing repetitive washing. After five cycles, the adsorption capacities of the adsorbent for Pb^{2+} and phenol separately decreased by 59.86% and 76.36%, implying that the prepared adsorbent can be used cyclically while the adsorption capacity did decrease. Compared with traditional adsorbents, the prepared adsorbent still exhibited good performance and can be used in wastewater treatment after being further optimised.

3.4. The Mechanism of Synergistic Effect. XPS is used to investigate the interaction between adsorbents and adsorbates. Figure 9 displays the XPS full-scan spectra before and after adsorption using NH_2-SH-GO/o-MWCNTs. As shown in Figure 9(a), there were characteristic peaks of five elements (C1s, O1s, Si2p, S2p, and N1s) in NH_2-SH-GO/o-MWCNTs before adsorption. However, a new peak (Pb4f) was seen in the NH_2-SH-GO/MWCNTs after adsorption, which suggested that Pb^{2+} was successfully adsorbed on the adsorbent. The characteristic peak of S2p shifted to a lower binding energy, implying that an interaction occurred between sulfhydryl in the adsorbent and adsorbates. Furthermore, the new characteristic peak of Pb4f was split (Figure 9(b)): $Pb4f_{7/2}$ and $Pb4f_{5/2}$ (two Gaussian energy spectra) separately occurred at 138.9 eV and 143.8 eV, which indicated that lead ions adsorbed on NH_2-SH-GO/o-MWCNTs were mainly divalent. As illustrated in Figure 9(c), the C1s energy spectrum of NH_2-SH-GO/o-MWCNTs can be decomposed into three Gaussian energy spectra. The Gaussian peaks appeared at 288.9, 286.4, and 284.6 eV and corresponded to C-OH in hydroxyl, C=O in carboxyl, and C-C functional groups in MWCNTs or GO, respectively. By analyzing the peaks of O1s in Figure 9(d), it can be seen that Gaussian peaks that occurred at 288.84, 286.52, and 284.68 eV corresponded to C-OH, C=O, and C-C, respectively. It was consistent with the analytical results arising from the energy spectra of C1s. These produced oxygen-containing groups directly demonstrated that surfaces of MWCNTs or GO had been successfully oxidized and they provided more adsorption sites for adsorbing lead ions and phenol. Figures 9(e) and 9(f) showed the Gaussian energy spectra of S2p before and after adsorption. It can be clearly seen from Figure 9(e) that the Gaussian peaks of S-H appeared at 169.1 and

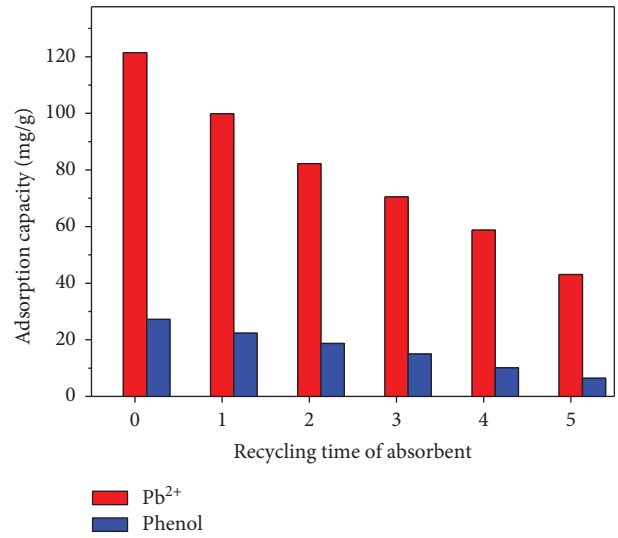

Figure 8: Influence of recycling times on adsorption capacity.

164 eV, which indicated that sulfhydryl groups were successfully loaded onto the NH_2-SH-GO/MWCNTs. However, the characteristic peak, at 169.1 eV, of NH_2-SH-GO/MWCNTs disappeared after the adsorbates were adsorbed, implying that sulfhydryl took part in this adsorption reaction and part of the –SH was damaged which reduced the peak area. The location of the characteristic peak of sulfhydryl did not change, which suggested that electron transfer did not occur in adsorption process (shown in Figure 9(f)).

Figures 9(g) and 9(h) separately display Gaussian energy spectra of N1s before and after adsorption. Figure 9(g) clearly suggested that a Gaussian peak of N-H occurred at 400.8 eV; however, the peak area of N-H group at 400.8 eV significantly decreased after adsorption and a new peak appeared at 404.1 eV. The new peak occurred because N-Pb bonds were formed through complexation between amino and Pb^{2+}. Occurrence of N-Pb bonds directly revealed that chemical bonds were formed by the chemical adsorption effect between the adsorbent and the adsorbates. Additionally, the reason why the binding energy increased was that nitrogen atoms provided a pair of electrons for the formation of N-Pb bonds during complexation, so the electron cloud density of nitrogen atoms decreased to increase the binding energy [32]. The results demonstrated that electrostatic interactions and complexation occurred in the adsorption process. According to the results of kinetic, adsorption model, and thermodynamic analyses, it can be seen that the adsorption process was a complex adsorption process which contained chemical and physical components.

Table 4 lists the types of elements and percentages of atoms in NH_2-SH-GO/o-MWCNTs. It can be speculated from the table that there were C, N, O, S, and Si elements in the NH_2-SH-GO/o-MWCNTs after adsorption and the atom percentages were 66.55%, 2.04%, 17.09%, 6.26%, and 6.78%, respectively. The high oxygen content indicated that numerous oxygen-containing groups were present on the surface of NH_2-SH-GO/o-MWCNTs, which also directly

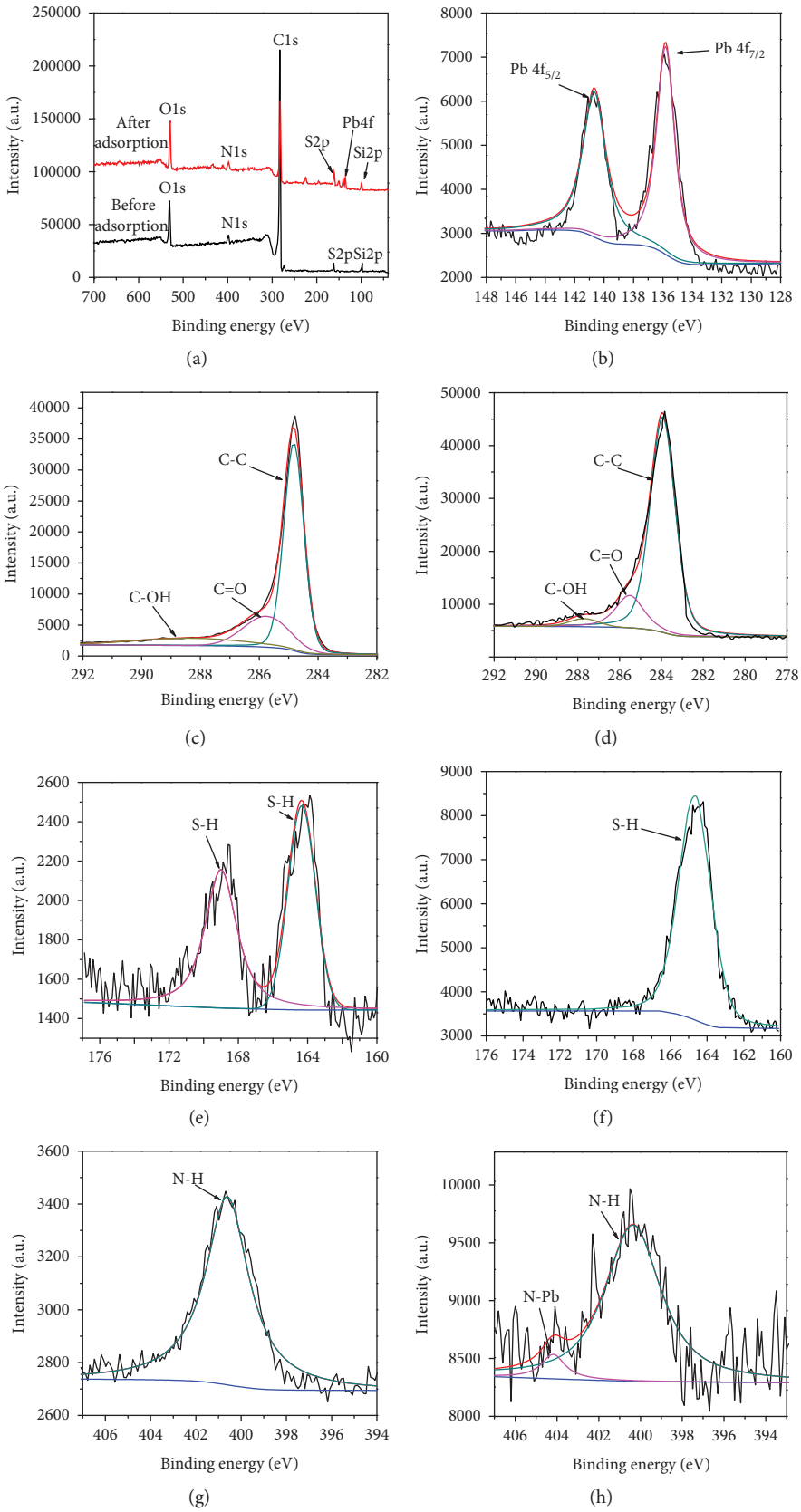

FIGURE 9: XPS spectra: before and after adsorption of NH_2-SH-GO/o-MWCNTs: (a) full spectrum of NH_2-SH-Fe_3O_4/o-MWCNTs; (b) Pb4f after adsorption; (c) C1S before adsorption; (d) C1S after adsorption; (e) S2p before adsorption; (f) S2p after adsorption; (g) N1s before adsorption; (h) N1s after adsorption.

Table 4: Element and atom contents of NH_2-SH-GO/o-MWCNTs.

Element	Peak value (eV)	Atomic content (%)
C1s		
Before	284.81	82.55
After	281.63	66.55
N1s		
Before	400.60	2.76
After	397.30	2.04
O1s		
Before	532.68	11.76
After	529.39	17.09
S2p		
Before	164.08	1.37
After	160.72	6.26
Si2p		
Before	102.85	1.56
After	99.38	6.78
Pb4f		
After	135.82	0.67

implied that there were many oxygen-containing groups on the surfaces of the MWCNTs or GO. Additionally, the proportions of C and N atoms in the NH_2-SH-GO/MWCNTs decreased after adsorption, indicating that an interaction occurred between amino and the adsorbates. Moreover, Pb4f appeared in the NH_2-SH-GO/MWCNTs after adsorption, which suggested that lead ions were adsorbed on the surface of the adsorbent.

4. Conclusion

The synergistic effect between magnetic field and NH_2-SH-GO/MWCNTs on scale inhibition and adsorption performance for Pb^{2+} and phenol at different temperatures was investigated. The NH_2-SH-GO/o-MWCNTs were first prepared. Additionally, changes in pH, conductivity, molecular activation energy, relative variations of intramolecular energy and the proportion of free water, and adsorption capacity of the adsorbent were studied under different temperatures. The results showed that with increasing initial temperatures, the molecular activation energies of circulating water grew while intramolecular energy did not undergo significant change. Moreover, the relative variation of the proportion of free water rose as well as the equilibrium adsorption capacities for Pb^{2+} and phenol. The equilibrium adsorption capacities for Pb^{2+} and phenol separately reached 131.27 mg/g and 35.79 mg/L at 40°C. The adsorption process for Pb^{2+} and phenol conformed to the pseudo-second-order kinetic model and Freundlich isotherm model. After five cycles, the adsorption capacities of the adsorbent for Pb^{2+} and phenol separately decreased by 59.86% and 76.36%. XPS results showed the adsorption process for Pb^{2+} and phenol was a complex adsorption process which contained chemical and physical components. The aforementioned results reveal that temperatures can promote the adsorption process for Pb^{2+} and phenol, showing potential for water treatment.

Data Availability

The data used to support the findings of this study are available from the corresponding author upon request.

Conflicts of Interest

The authors declare that there are no competing interests regarding the publication of this paper.

Acknowledgments

The authors are grateful for the financial support received from the National Natural Science Foundation of China (51304101, 51764039), Youth Science and Technology Fund Project of Gansu Province (1606RJYA305, 17JR5RA116) and doctor research cost of Lanzhou University of Technology (061702).

References

[1] P. Gao, G. Xue, X. S. Song, and Z. H. Liu, "Depth filtration using novel fiber-ball filter media for the treatment of high-turbidity surface water," *Separation and Purification Technology*, vol. 95, no. 19, pp. 32–38, 2012.

[2] L. D. Tijing, D. H. Lee, D. W. Kim, Y. I. Cho, and C. S. Kim, "Effect of high-frequency electric fields on calcium carbonate scaling," *Desalination*, vol. 279, no. 1–3, pp. 47–53, 2011.

[3] V. Arulmozhi and A. S. Rao, "Proton magnetic resonance relaxation studies in aqueous solutions of alkali halides and sugars," *Physics and Chemistry of Liquids*, vol. 26, no. 3, pp. 201–207, 1993.

[4] R. A. Horne and D. S. Johnson, "The viscosity of water under pressure," *Journal of Physical Chemistry*, vol. 70, no. 7, pp. 2182–2190, 1966.

[5] R. Li, Z. Jiang, S. Shi, and H. Yang, "Raman spectra and ^{17}O NMR study effects of $CaCl_2$ and $MgCl_2$ on water structure," *Journal of Molecular Structure*, vol. 645, no. 1, pp. 69–75, 2003.

[6] L. Jiang, C. Li, H. Yu, Z. Zou, F. Shen, and X. Hou, "Preparation of NH_2-SH-GO/MWCNTs composite for simultaneous removal of Pb(II), Zn(II) and phenol from aqueous solution," *Desalination and Water Treatment*, vol. 97, pp. 272–284, 2017.

[7] J.-D. Zhao, Z.-A. Liu, and E.-J. Zhao, "Combined effect of constant high voltage electrostatic field and variable frequency pulsed electromagnetic field on the morphology of calcium carbonate scale in circulating cooling water systems," *Water Science & Technology*, vol. 70, no. 6, pp. 1074–1082, 2014.

[8] H. Wang, W. Wang, Y. Zhao et al., "Superior adsorption of 3D nanoporous architectures for Ni(II) ions adsorption using polyvinyl alcohol as cross-linking agent and adsorption conveyor," *RSC Advances*, vol. 8, no. 15, pp. 7899–7903, 2018.

[9] F. Wang, Y. Wang, and Y. Li, "Preparation of 6-diallylamino-1, 3, 5-triazine-2, 4-disulfydryl functional nanofilm by electrochemical polymerization technique on aluminum surface," *International Journal of Electrochemical Science*, vol. 6, pp. 793–803, 2016.

[10] M. Gryta, "The influence of magnetic water treatment on CaCO3 scale formation in membrane distillation process," *Separation and Purification Technology*, vol. 80, no. 2, pp. 293–299, 2011.

[11] Z. J. Dong, J. B. Yan, H. B. Tu, Z. K. Song, and X. X. Fan, "Studying on the preparation and application of silica aerogel composites for thermal insulation," *New Chemical Materials*, vol. 33, no. 3, pp. 46–48, 2005.

[12] Y.-H. Li, S. Wang, Z. Luan, J. Ding, C. Xu, and D. Wu, "Adsorption of cadmium (II) from aqueous solution by surface oxidized carbon nanotubes," *Carbon*, vol. 41, no. 5, pp. 1057–1062, 2003.

[13] T. A. Saleh and V. K. Gupta, "Column with CNT/magnesium oxide composite for lead (II) removal from water," *Environmental Science and Pollution Research*, vol. 19, no. 4, pp. 1224–1228, 2012.

[14] M. Hadavifar, N. Bahramifar, H. Younesi, and Q. Li, "Adsorption of mercury ions from synthetic and real wastewater aqueous solution by functionalized multi-walled carbon nanotube with both amino and thiolated groups," *Chemical Engineering Journal*, vol. 237, pp. 217–228, 2014.

[15] L. Jiang, H. Yu, X. Zhou et al., "Preparation, characterization, and adsorption properties of magnetic multi-walled carbon nanotubes for simultaneous removal of lead (II) and zinc (II) from aqueous solutions," *Desalination and Water Treatment*, vol. 57, no. 39, pp. 18446–18462, 2015.

[16] B. Mahmoud, M. Yosra, and A. Nadia, "Effects of magnetic treatment on scaling power of hard waters," *Separation and Purification Technology*, vol. 171, pp. 88–92, 2016.

[17] G. Li, W. Zhu, C. Zhang et al., "Effect of a magnetic field on the adsorptive removal of methylene blue onto wheat straw biochar," *Bioresource Technology*, vol. 206, pp. 16–22, 2016.

[18] C. Zhang, J. Sui, J. Li, Y. Tang, and W. Cai, "Efficient removal of heavy metal ions by thiol-functionalized superparamagnetic carbon nanotubes," *Chemical Engineering Journal*, vol. 210, pp. 45–52, 2012.

[19] L. Jiang, X. Yao, H. Yu et al., "Effect of permanent magnetic field on scale inhibition property of circulating water," *Water Science and Technology*, vol. 76, no. 8, pp. 1981–1991, 2017.

[20] S. Kumar and N. Krishnamurthy, "Variation of activation energy of hydrogen absorption of vanadium as a function of aluminum," *International Journal of Hydrogen Energy*, vol. 37, no. 18, pp. 13429–13436, 2012.

[21] J. Emsley, M. Arif, P. A. Bates, and M. B. Hursthouse, "Hydrogen bonding between free fluoride ions and water molecules: two X-ray structures," *Journal of Molecular Structure*, vol. 220, no. 220, pp. 1–12, 1990.

[22] Y.-X. Ma, D. Xing, W.-J. Shao, X.-Y. Du, and P.-Q. La, "Preparation of polyamidoamine dendrimers functionalized magnetic graphene oxide for the adsorption of Hg(II) in aqueous solution," *Journal of Colloid and Interface Science*, vol. 505, pp. 352–363, 2017.

[23] P. A. M. Mourão, C. Laginhas, F. Custódio, J. M. V. Nabais, P. J. M. Carrott, and M. M. L. R. Carrott, "Influence of oxidation process on the adsorption capacity of activated carbons from lignocellulosic precursors," *Fuel Processing Technology*, vol. 92, no. 2, pp. 241–246, 2011.

[24] Y. Ma, P. La, W. Lei, C. Lu, and X. Du, "Adsorption of Hg(II) from aqueous solution using amino-functionalized graphite nanosheets decorated with Fe_3O_4 nanoparticles," *Desalination and Water Treatment*, vol. 57, no. 11, pp. 5004–5012, 2015.

[25] K. Nithya, A. Sathish, P. Senthil Kumar, and T. Ramachandran, "Fast kinetics and high adsorption capacity of green extract capped superparamagnetic iron oxide nanoparticles for the adsorption of Ni(II) ions," *Journal of Industrial & Engineering Chemistry*, vol. 59, pp. 230–241, 2018.

[26] C. T. Li and S. L. Zhu, "Research on phenol waste water treatment by electrochemical oxidation," *Electrochemistry*, vol. 11, no. 1, pp. 101–103, 2005.

[27] G. Crini and P. M. Badot, "Application of chitosan, a natural aminopolysaccharide, for dye removal from aqueous solutions by adsorption processes using batch studies: a review of recent literature," *Progress in Polymer Science*, vol. 33, no. 4, pp. 399–447, 2008.

[28] R. Touir, M. Cenoui, M. El Bakri, and M. Ebn Touhami, "Sodium gluconate as corrosion and scale inhibitor of ordinary steel in simulated cooling water," *Corrosion Science*, vol. 50, no. 6, pp. 1530–1537, 2008.

[29] R. Cai, H. Yang, J. He, and W. Zhu, "The effects of magnetic fields on water molecular hydrogen bonds," *Journal of Molecular Structure*, vol. 938, no. 1–3, pp. 15–19, 2009.

[30] L. Fan, C. Luo, M. Sun, X. Li, and H. Qiu, "Highly selective adsorption of lead ions by water-dispersible magnetic chitosan/graphene oxide composites," *Colloids and Surfaces. B, Biointerfaces*, vol. 103, no. 1, pp. 523–529, 2013.

[31] K. Karthick, C. Namasivayam, and L. A. Pragasan, "Kinetics and isotherm studies on acid dye adsorption using thermal and chemical activated *Jatropha* husk carbons," *Environmental Progress & Sustainable Energy*, vol. 37, no. 2, pp. 719–732, 2018.

[32] R. Fu, Y. Liu, Z. Lou, Z. Wang, S. A. Baig, and X. Xu, "Adsorptive removal of Pb (II) by magnetic activated carbon incorporated with amino groups from aqueous solutions," *Journal of the Taiwan Institute of Chemical Engineers*, vol. 62, pp. 247–258, 2016.